

# A Study on Stroke Rehabilitation through Task-Oriented Control of a Haptic Device via Near-Infrared Spectroscopy-Based BCI

Berdakh Abibullaev, Jinung An, Seung-Hyun Lee, and Jeon-II Moon

**Abstract**—This paper presents a study in task-oriented approach to stroke rehabilitation by controlling a haptic device via near-infrared spectroscopy-based brain-computer interface (BCI). The task is to command the haptic device to move in opposing directions of leftward and rightward movement. Our study consists of data acquisition, signal preprocessing, and classification. In data acquisition, we conduct experiments based on two different mental tasks: one on pure motor imagery, and another on combined motor imagery and action observation. The experiments were conducted in both offline and online modes. In the signal preprocessing, we use localization method to eliminate channels that are irrelevant to the mental task, as well as perform feature extraction for subsequent classification. We propose multiple support vector machine classifiers with a majority-voting scheme for improved classification results. And lastly, we present test results to demonstrate the efficacy of our proposed approach to possible stroke rehabilitation practice.

**Index Terms**—Stroke rehabilitation, brain-computer interface, non-invasive, task-oriented, near-infrared spectroscopy, haptic device, offline and online classification, principal component analysis, multiple support vector machines, channel localization

## I. INTRODUCTION

Recent rehabilitation methods utilize brain-computer interface (BCI) to induce brain plasticity for motor control, or achieve some degree of patient self-sufficiency by commanding through thinking [1]. This approach gained heightened interest in the research community and opened new possibilities for a considerable number of medical applications. However, there is still a significant work to be performed before this technology can be fully used in practice, as there is still no overwhelming evidence of functional recovery on stroke rehabilitation through BCI [2].

This paper presents a task-oriented training for on-line stroke rehabilitation by controlling a haptic device through leftward and rightward movement via near-infrared spectroscopy (NIRS)-BCI [3], as shown in Fig. 1. This emerging modality of non-invasive BCI [4], [5] measures the cortical hemodynamics and oxygenation status through chromophore concentration levels of oxyhemoglobin (oxy-Hb) and deoxyhemoglobin (deoxy-Hb) [6],[7], [8], [9].

B. Abibullaev, J. An, J.I. Moon, and S.H. Lee are with the Robotics Research Division. All are with Daegu-Gyeongbuk Institute of Science & Technology, 50-1 Sangri, Hyeonpung-Myeon, Dalseong-gun, Daegu, 711-873, Republic of Korea. E-mail: {berdakho}@dgist.ac.kr.

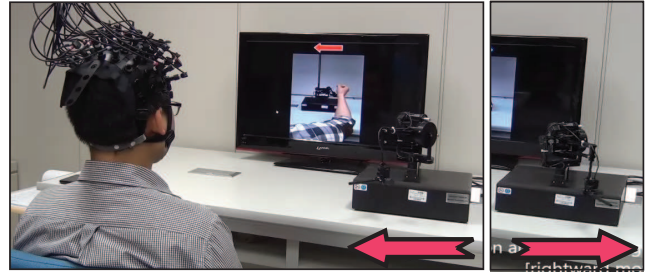


Fig. 1. A subject commands the haptic device to move rightward and leftward through commands generated by his brain signals and read through near-infrared spectroscopy-BCI. This experiment is performed based on both motor imagery and action observation. A demonstration video of performed experiments is shown here: [http://youtu.be/bYdJWdPn\\_LI](http://youtu.be/bYdJWdPn_LI).

BCI-based rehabilitation has been the focus of many literature studies which include studies of its different aspects on signal, control, and usage [10]; interactive feedback and control strategies [11], [12]; progress of rehabilitation strategies [13]; motor imagery to facilitate rehabilitation [14]; and implications of BCI to rehabilitation [15].

More recent literature studies looked into virtual reality and its applications to neuroscience research for neurorehabilitation [16]; BCI in communication [17], motor control and neural activities [18]; its dependence on signal acquisition, validation to real-world use, and reliability of function [19]; and recovery of hand motor function [20].

A considerable number of experiments related to BCI-based rehabilitation have been conducted. These include minimal training and mental stress to patient [21], rehabilitative intervention for hand plegia [22], control of 9-degrees-of-freedom (DOF) wheelchair-mounted robotic arm [23], and virtual environment to facilitate neuroplasticity [24]. More recent experiments include detection of movement intention [25], exoskeleton to control fingers with feedback [26], removing artifact in motor imagery [27], calibrating imagery through passive movement [28], studying motor learning after stroke [29], and test of feasibility of single-trial, individually-tuned classifiers [30].

Despite the above efforts, only a few BCI-based rehabilitation studies have included a haptic device in their approach. Interestingly, there are empirical evidences that tactile sensing through haptic feedback [31] and vibrotactile stimulus [32] show improved rehabilitation results. Our work aims to contribute to the same efforts of including haptic device to BCI-based rehabilitation, and is

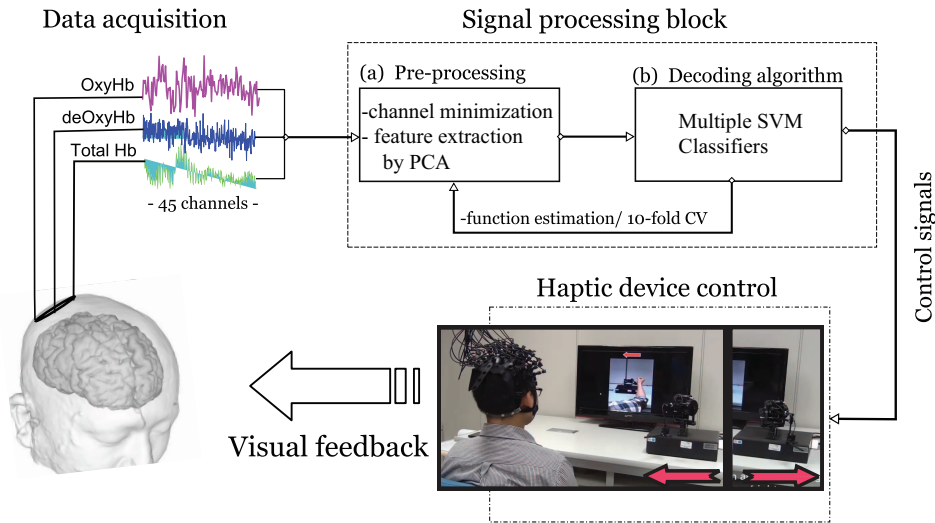


Fig. 2. Flowchart of the task-oriented control of a haptic device via NIRS-BCI. Concentrations of oxy-Hb and deoxy-Hb are read from 45-channel of NIRS. Input signals are pre-processed by identifying the more significant channels, and by performing feature extraction through principal component analysis (PCA). Classification is performed via multiple support vector machines (SVMs), whose output is also used for tenfold cross validation (CV). The decoded outputs are then used to control movements of an external haptic device in either leftward or rightward motion. Success or failure of the task required is determined through the visual feedback of the haptic motion.

implemented by using both motor imagery and combined motor imagery-action observation methods. To drive the haptic device, signals are pre-processed and most significant channels are identified, then the output signals are classified to move the haptic device to a desired direction. Visual feedback determines the success or failure of the desired action based on the subject's brain signal command. Our experimental setup will be described and results of training the classifier will be shown. Online and offline test results will be presented which determines the efficacy of our proposed method for stroke rehabilitation.

This work proceeds as follows. Section II presents how our classifiers are trained and optimized through offline supervised learning. Once these classifiers are optimized, we test them with offline and online data sets. The offline test data results are shown in Section III, while the more challenging case of testing via online data streaming is shown in Section IV. And lastly, Section V shows the discussion and comparison between our results and the previously published results in BCI-based rehabilitation.

## II. MATERIALS AND METHODS

Offline supervised learning is used to train and optimize our classifiers. First, raw signals are pre-processed using feature extraction through principal component analysis (PCA). This reduces the noise from the raw signal that was read through NIRS-BCI. Furthermore, more significant channels of NIRS-BCI are identified through recursive channel elimination (RCE). This eliminates the non-task-relevant channels, which can be another source of signal noise. From the processed signals that were read through task-relevant channels, classification is performed based on the actions commanded by the subject. Our classification uses multiple support vector machines (SVMs), where a majority voting mechanism is then used to further refine

the classification process. Output from SVMs is used for tenfold cross validation (CV) in the signal pre-processing stage. Test data from both offline and online data sets verifies the efficacy of the trained classifiers. The flowchart of the entire experimental process is shown in Fig. 2.

### A. Data Acquisition

Experimental subjects consist of seven healthy, right-handed males ages  $28 \pm 4$  years. All study participants gave informed consent. The ethical approval of the research was granted by the research ethics committees of the Daegu-Gyeongbuk Institute of Science and Technology.

The NIRS-BCI used in our work has 45-channel optical brain-function imaging system for data acquisition (FOIRE-3000, Shimadzu Co. Ltd., Japan). It uses safe near-infrared light to assess the oxy-Hb and deoxy-Hb concentrations of the brain at wavelengths of 780 nm, 805 nm, and 830 nm. This study uses concentration levels of oxy-Hb for analysis and classification, which are found to be more correlated with the regional cerebral blood flow (rCBF) than deoxy-Hb and total-Hb [33]. An increase in rCBF reflects an increase in neural activity [34].

We placed the optical fiber probes on the frontoparietal regions of the brain cortex to cover an area of  $21 \times 12$  cm as shown in Fig. 3A. The subjects performed three types of mental tasks denoted by  $\{t_{right}\}$ ,  $\{t_{left}\}$  and  $\{t_{rest}\}$  as follows:

- $\{t_{right}\}$  - subjects repetitively performed an imaginary rightward movement of the haptic device,
- $\{t_{left}\}$  - subjects repetitively performed an imaginary leftward movement of the haptic device, and
- $\{t_{rest}\}$  - subjects rest and perform no actual task.

The signals during rest were used as the baseline in a classification process. Each subject performed five-session mental tasks for a total of 35 sessions for all subjects. We

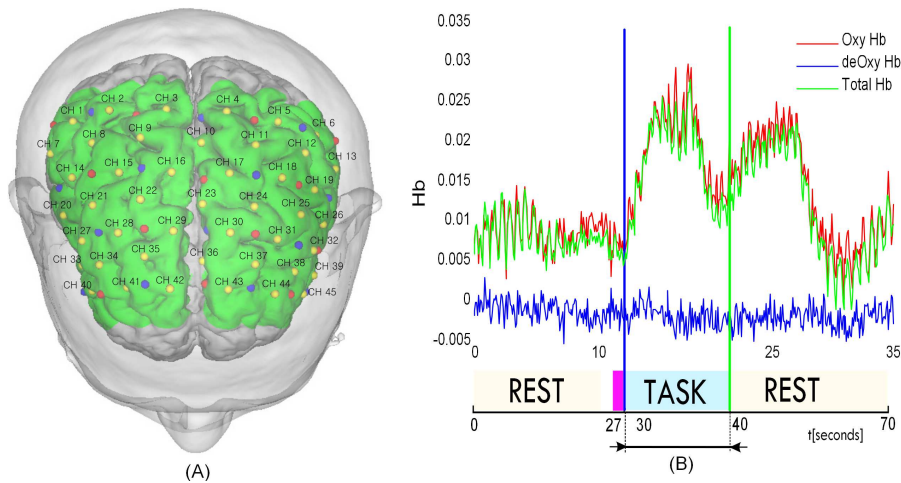


Fig. 3. (A) The locations of NIRS emitter-receiver optodes with 30-mm interoptode distance. The red circles represent emitters and blue circles represent receivers. The yellow circles represent the locations of the 45 channels recorded. (B) The timing of a single experimental trial of data acquisition, shown with its corresponding oxy-Hb, deoxy-Hb, and total Hb concentrations at each stage of the task.

split every session into three blocks [*Rest*  $\rightarrow$  *Task*  $\rightarrow$  *Rest*] as shown in Fig. 3B. In the same figure, the corresponding levels of oxy-Hb, deoxy-Hb, and total Hb are also shown during one experimental session of MI task.

### B. Types of Experiments

This work uses two types of tasks to control the haptic device: 1.) motor imagery (MI) task, and 2.) a combined action observation (AO) and MI tasks. The latter type of task is also referred to as AOMI task.

In MI tasks, subjects merely imagine the task without an external cue. In AOMI tasks, the subject performs an AO task followed by an MI task. The AO task consists of watching a video that shows the movements of a subject's forearm in the intended direction. Our motivation for the AOMI task experiment is based on earlier studies related to the putative human mirror neuron system that describe how predictions and interpretations of the actions of others were exploited for BCI systems [35] [36]. We want to investigate whether the combined AOMI task provides higher BCI classification rates than a pure MI task.

### C. Signal Pre-processing

We consider two significant factors that affect the accuracy of a BCI system: 1.) background noise, and 2.) task-irrelevant channels.

The noise interference in hemodynamic signals may arise from instrumental, experimental, or physiological sources. Particularly, physiological noise often overlap in frequency with the expected neural signals [3]. In this study, we employ PCA for noise reduction and feature extraction, which has shown to be more reliable in eliminating background noises in NIRS signals [37]. Other noise-reduction methods use Weiner filtering [38], wavelets [39], [40], and adaptive filtering [6].

Selecting task-relevant channels may yield the required accuracy with greater convenience [41], [42]. Unfortunately, optimal channel selection is not a trivial task, in

particular for NIRS-BCI, when extracting neurophysiologic knowledge corresponding to a specific mental task. The next section describes our BCI channel selection strategy in more detail.

### D. Principal Component Analysis

The neural datasets are denoted by  $X \in R^{l \times m}$ , such that  $l$  is the number of channels and  $m$  is the number of samples. We denote a single trial dataset as a matrix  $X \in R^{l \times m}$  that has its rows  $\{x_1, x_2, \dots, x_l\}^T$  composed of the channel observations with  $m$  features or dimensions. Our goal is to find a new data matrix  $X \in R^{l \times k}$  where  $k < m$ .

We employ a PCA method for this purpose. It is based on projecting signal features  $x \in R^m$  onto a subspace defined by a set of orthonormal vectors  $u \in R^m$  that maximize the data variance  $E$ ,

$$\begin{aligned} & \text{maximize } E = u^T X^T X u & (1) \\ & \text{subject to } \|u\| = 1 \end{aligned}$$

Solving the optimization in Eq. 1 by the Lagrangian method yields the eigenvalue equation  $X^T X u = \lambda u$ . It follows that to maximize the variance, the chosen  $u$  must be the eigenvector of  $X^T X$  corresponding to the largest eigenvalue. In order to compute  $k$  directions, we must find eigenvectors  $u_1, \dots, u_k$  corresponding to the  $k$  largest eigenvalues given  $\lambda_1, \dots, \lambda_k$ , such that  $\lambda_1 \geq \lambda_2 \geq \dots \geq \lambda_k$ . Algorithm 1 shows our method to find the PCA projection directions. The resulting features extracted by PCA are  $X u_1, \dots, X u_k$ .

### E. Recursive Channel Elimination

We employ a recursive channel elimination (RCE) algorithm [41],[43] for identifying the recording positions most relevant to cognitive tasks. The method is based on recursive feature elimination [44], which is an iterative, embedded, greedy backward method of feature selection. The best channels are determined by training several SVMs

**Algorithm 1: PCA Pre-processing**


---

1 **Input:** Data matrix  $X^{l \times m}$ , dimension  $k$   
2 Process:  $X_1 = X$ ;  
3 **foreach**  $i = 1, \dots, k$  **do**  
4     Select  $u_j$  as the first eigenvector of  $X_i^T X_j$ ;  
5      $X_{j+1} = X_j \left( I - \frac{u_j u_j^T}{u_j^T u_j} \right)$   
6 **Output:** Projection directions  $u$  and features  $Xu$

---

and exploring their marginal characteristics. Algorithm 2 describes our method for channel selection. The algorithm can be summarized as follows:

- make ten disjoint training datasets (Line 2) for tenfold CV,
- train a linear SVM (Line 9) and estimate the generalization error (Line 10) for each fold,
- estimate the rank of the channels based on a margin ranking criterion (Lines 11-14), and
- eliminate channels with the lowest ranking score criterion (Line 15).

We repeat the procedure until the required number of channels is retained throughout all ten datasets. We define a threshold value for the number of channels that potentially need to be retained. This is done by trial and error on the basis of the test error rate at Line 10. We tried several channel combinations and decided to select only 20 of the 45 channels for subsequent classification.

**Algorithm 2: Recursive Channel Elimination**


---

1 **Input:**  $\{x_i, y_i\}_{i=1}^l$ ,  $x_i \in X$ ,  $y_i \in \{\pm 1\}$ , training set with  $l$  channels related to either  $\{t_{right}\}$  or  $\{t_{left}\}$  tasks.  
2 Perform tenfold, divide the training set (of size)  $m$  into  $p$  disjoint sets  $S_j, \dots, S_p$  of equal size  $p/m$ ;  
3 **foreach**  $S_j$  **do**  
4     Initialize:  $Ranked = [\emptyset]$ ;  
5     Surviving channels  $Ch_j = [1, 2, \dots, l]$   
6     **while** *Surviving channel is not empty* **do**  
7         **foreach** *channel in*  $Ch_j = [1, 2, \dots, l]$  **do**  
8             Temporarily remove channel  $j$  in  $Ch_{(j=1, \dots, l)}$ ;  
9             Train a linear SVM with the remaining channels of  $S/S_j$  and estimate  $|w|$  (from Eq. 2, Eq. 3);  
10             Test it on  $S_j \mapsto \{\pm 1\}$ ;  
11             Compute the ranking score:  
12              $R_j = \frac{1}{|Ch_j|} \sum_{l \in Ch_j} |w_l|$ ;  
13             Locate channels with smallest ranking criterion:  $RankChan = \operatorname{argmin}\{R_j\}$ ;  
14             Update channel rank:  
15              $Ranked = [RankChan, Ranked]$ ;  
16             Eliminate the channel with smallest  $R_j$  score;  
17         **end foreach**  
18     **end while**  
19     **end foreach**  
20 **Output:** Extracted channel list:  $Ranked$

---

**F. Classification**

Given set of pre-processed training dataset  $X := \{x_1, \dots, x_m\}$  with corresponding labels  $Y := \{y_1, \dots, y_m\}$ , where  $y_i \in \{\pm 1\}$  for  $i = 1, \dots, m$ , our next goal is to estimate a function  $f : X \rightarrow \{\pm 1\}$  to predict whether a new signal observation  $z \in X^*$  will belong to class +1 or -1. We defined the classes for the mental tasks  $[\{t_{right}, +1\}, \{t_{rest}, -1\}]$  as patterns related to rightward movement ( $y = +1$ ) and the baseline ( $y = -1$ ). Similarly, we define  $[\{t_{left}, +1\}, \{t_{rest}, -1\}]$  as patterns related to leftward movement and the baseline ( $y = -1$ ). We estimate a set of SVM functions for classification with a soft margin loss function  $L(x, y, f(x)) = \max(0, 1 - yf(x))$ .

The solution of SVM is based on the following optimization [45]:

$$\begin{aligned} \min_{\alpha \in R, b \in R} \left\{ \frac{1}{C} \sum_{i=1}^m \xi_i + \sum_{i,j=1}^m \alpha_i y_i K(x_i, z_j) \alpha_j y_j \right\} \\ \text{subject to } y_j \left( \sum_{i=1}^m \alpha_i y_i K(x_i, z_j) + b \right) \geq 1 - \xi_i \\ \xi_i \geq 0, \forall i = 1, 2, \dots, n \end{aligned} \quad (2)$$

where  $\alpha = (\alpha_1, \dots, \alpha_m)$  are Lagrange multipliers, the  $\xi_i$  are slack variables and a user defined regularization parameter  $C > 0$ . The corresponding decision function is given by,

$$f(z) = \operatorname{sign} \left[ \left( \sum_{i=1}^m \alpha_i y_i K(x_i, z) \right) + b \right]. \quad (3)$$

From Eq.2 and Eq. 3, the  $K(x, z)$  is a reproducing kernel function which gives rise to a Gram matrix  $K_{i,j} := (x_i, z_j)$ ,  $K \in R^{m \times m}$  [20]. This matrix contains all the information available in order to perform data analysis and modeling of SVM algorithm. Note that we use this formulation of the SVM for two different purposes. First, we use SVMs for the recursive channel elimination method in Algorithm 2. Second, SVMs constitute the bases functions of multiple classifiers which we use for decoding of signal features related to MI and AOMI tasks.

**G. Multiple SVM Classifiers**

Instead of training a single classifier, we study train multiple SVMs with the purpose of further improving the overall BCI accuracy. We consider a multiple  $n$  - classifier functions  $\{f_1, f_2, \dots, f_n\}$  and a data set  $\{(x_i, y_i)_{i=1}^m\}$ ,  $x_i \in X$ ,  $y_i \in Y$ . Each classifier is trained independently to predict  $f_{i=1}^n : x \rightarrow \{\pm 1\}^n$ . The outputs from all classifier functions are then defined as an  $m$ -dimensional binary vector  $y = [y_{1,i}, \dots, y_{m,i}]$ , such that  $y_{j,i} = 1$  if  $f_i$  recognizes  $x_j$  and 0 otherwise for  $i = 1, \dots, n$ .

Table 1 shows that the number of correct assignments is  $N_1(f_i) = \sum_{j=1}^m y_{j,i}$  and the number of mistakes is  $N_0(f_i) = m - \sum_{j=1}^m y_{j,i}$ . In order to make the final decision from the set of functions  $\{f_i, \dots, f_n\}$ , we define

---

**Algorithm 3: Multiple SVM Training and Testing**


---

```

1 Define:  $\mathcal{E}_1 = \{f_1, \dots, f_6\}$  and  $\mathcal{E}_2 = \{f_1^*, \dots, f_6^*\}$ ;
2 Input:  $\{x_i, y_i\}_{i=1}^m$ ,  $x_i \in X$ ,  $y_i \in \{\pm 1\}$ , training set
   related to either  $\{t_{right}\}$  or  $\{t_{left}\}$  mental
   tasks.
3 foreach  $f_i \in \mathcal{E}_1$  or  $f_j^* \in \mathcal{E}_2$ ,  $i, j = 1, \dots, 6$  do
4   Perform tenfold CV and a search on optimal  $C$ ;
5   Divide the training set (of size)  $m$  into  $p$  disjoint
   sets  $S_j, \dots, S_p$  of equal size  $p/m$ ;
6   foreach  $S_j$  do
7     Train a  $f_i(x)$  on  $S/S_j$ ;
8     Test it on  $S_j \mapsto AUC(j)$ ;
9     Output: Optimized classifier model :  $f(\cdot, \alpha, b)$ 
10 Output: Set of optimized
     $\mathcal{E}_1 = \{f_1(\cdot, \alpha_1), \dots, f_6(\cdot, \alpha_6)\}$ 
     $\mathcal{E}_2 = \{f_1^*(\cdot, \alpha_1), \dots, f_6^*(\cdot, \alpha_6)\}$ .
11 Input:  $\{z_i\}_{i=1}^n$ ,  $z_i \in X$  unseen test patterns related to
    either  $\{t_{right}\}$  or  $\{t_{left}\}$  mental tasks.
12 foreach  $f_i(\cdot, \alpha_i) \in \mathcal{E}_1$  or  $f_j^*(\cdot, \alpha_j) \in \mathcal{E}_2$ ,  $i, j = 1, \dots, 6$ 
    do
13   Evaluate  $\mathcal{E}$ :  $f_i(x_j, \alpha_i) \rightarrow y_{N,l}$ , where  $y_{j,i} \in \{\pm 1\}$ 
    are the columns of Table 1,  $i = 1, \dots, l$  classifiers
    and  $j = 1, \dots, n$  test patterns;
14   (1)-Majority vote: define  $k$ -of- $l$  majority voting
    classifiers as defined in Eq. 4.;
15   (2)-Output: compute the final AUC value for
    majority classifiers  $\mathcal{E} \rightarrow AUC$ ;
16 Output:  $\mathcal{E}_1 \rightarrow AUC_1$  and  $\mathcal{E}_2 \rightarrow AUC_2$ 

```

---

the following majority voting rule:

$$F(z) = \begin{cases} +1 & \text{if } \sum_i^n f_i(z) \geq k \\ -1 & \text{else } \sum_i^l f_i(z) \leq n - k \\ U & \text{Otherwise} \end{cases} \quad (4)$$

where  $k < n$  and  $i = 1, \dots, k$  making similar predictions defined by the  $k$ -of- $n$  majority classifier for  $k \geq \frac{n}{2}$ . In this case,  $U$  represents the unknown outputs or failure in predicting both outputs. Thus, we have three possible outcomes from all classifiers  $F : X \rightarrow \{+1, -1, U\}$ .

Algorithm3 gives the details of the proposed multiple SVM classifier training and validation sequentially. This consists of two main phases, namely, the training phase and the testing phase. In both phases, we train and test two different group of multiple classifiers  $\mathcal{E}_1$  and  $\mathcal{E}_2$ .

TABLE I  
STRUCTURE OF MULTIPLE OUTPUTS

	$f_1$	$\dots$	$f_i$	$\dots$	$f_n$
$x_1$	$y_{1,1}$	$\dots$	$y_{1,i}$	$\dots$	$y_{1,n}$
$\vdots$	$\vdots$		$\vdots$		$\vdots$
$x_j$	$y_{j,1}$	$\dots$	$y_{j,i}$	$\dots$	$y_{j,n}$
$\vdots$	$\vdots$		$\vdots$		$\vdots$
$x_m$	$y_{m,1}$	$\dots$	$y_{m,i}$	$\dots$	$y_{m,n}$

The group  $\mathcal{E}_1$  is trained by taking the examples from rightward task  $\{t_{right}\}$  as positive and the examples from the rest task  $\{t_{rest}\}$  as negative. Likewise, the group  $\mathcal{E}_2$  is trained by taking the examples from the leftward task  $\{t_{left}\}$  as positive and the examples from the rest task  $\{t_{rest}\}$  as negative. Each group consists of six base SVM functions with linear kernels.

In the training phase, each individual base SVM function is trained separately using the same input data from the tenfold CV (Algorithm 3, Lines 1-9).

During the testing phase, unseen examples are applied to all base functions simultaneously in real time. Further, a collective decision is obtained on the basis of the majority voting scheme using Eq. 4 (Algorithm 3, Lines 12-16). In other words, once each of the six base classifiers has cast its vote, the majority voting strategy assigns the test patterns to the class with the largest number of votes and outputs are provided as the final prediction.

Then, the final decision on which direction to move the haptic device with the output control command is based on the area under the receiver operating characteristic (ROC) curve. This area under the ROC curve is also referred to as AUC. The AUC is a comparatively robust measure that is insensitive to class distributions and misclassification costs [46]. For instance,  $AUC = 1$  indicates perfect classification, whereas  $AUC = 0.5$  indicates that the result from the classifier is no better than a random guess. In our case, an  $AUC > 0.70$  moves the haptic device to the desired direction.

### III. OFFLINE TEST RESULTS AND ANALYSIS

For each of the seven subjects, we trained subject-specific multiple SVM classifiers (Algorithm 3) with an input dataset consisting of 20 channels selected using the RCE algorithm. The relevant channel locations varied among subjects and sessions, and were updated every time a subject performs mental tasks. The search for an optimal penalty parameter was conducted to obtain the best CV performance. Then we gathered offline data set to test the performance of our resulting classifier. The resulting UAC values are shown in Fig. 4 in moving the haptic device in rightward and leftward direction, in both MI and AOMI task commands. We assign  $AUC > 0.70$  to be acceptable, such that the haptic device is moved to the desired direction.

For the sake of discussion, we introduce the following three classifier performance regions:

- $\Theta_{best} := (0.80, \dots, 1]$ , if  $AUC \geq 0.80$ ,
- $\Theta_{accept} := (0.70, \dots, 0.80]$ , if  $0.70 < AUC \leq 0.80$ ,
- $\Theta_{worst} := (0.60, \dots, 0.70]$ , if  $0.60 < AUC \leq 0.70$ .

The haptic system is the PHANTOM Premium 1.0 haptic device (19.5 cm  $\times$  27 cm  $\times$  37.5 cm workspace, two active degrees of freedom). Real-time neural data were acquired through a LabVIEW - NIRS interface, wherein the proposed algorithms were implemented.

Let us consider the decoding results of MI task commands in Figs. 4A (rightward movement) and 4B (leftward

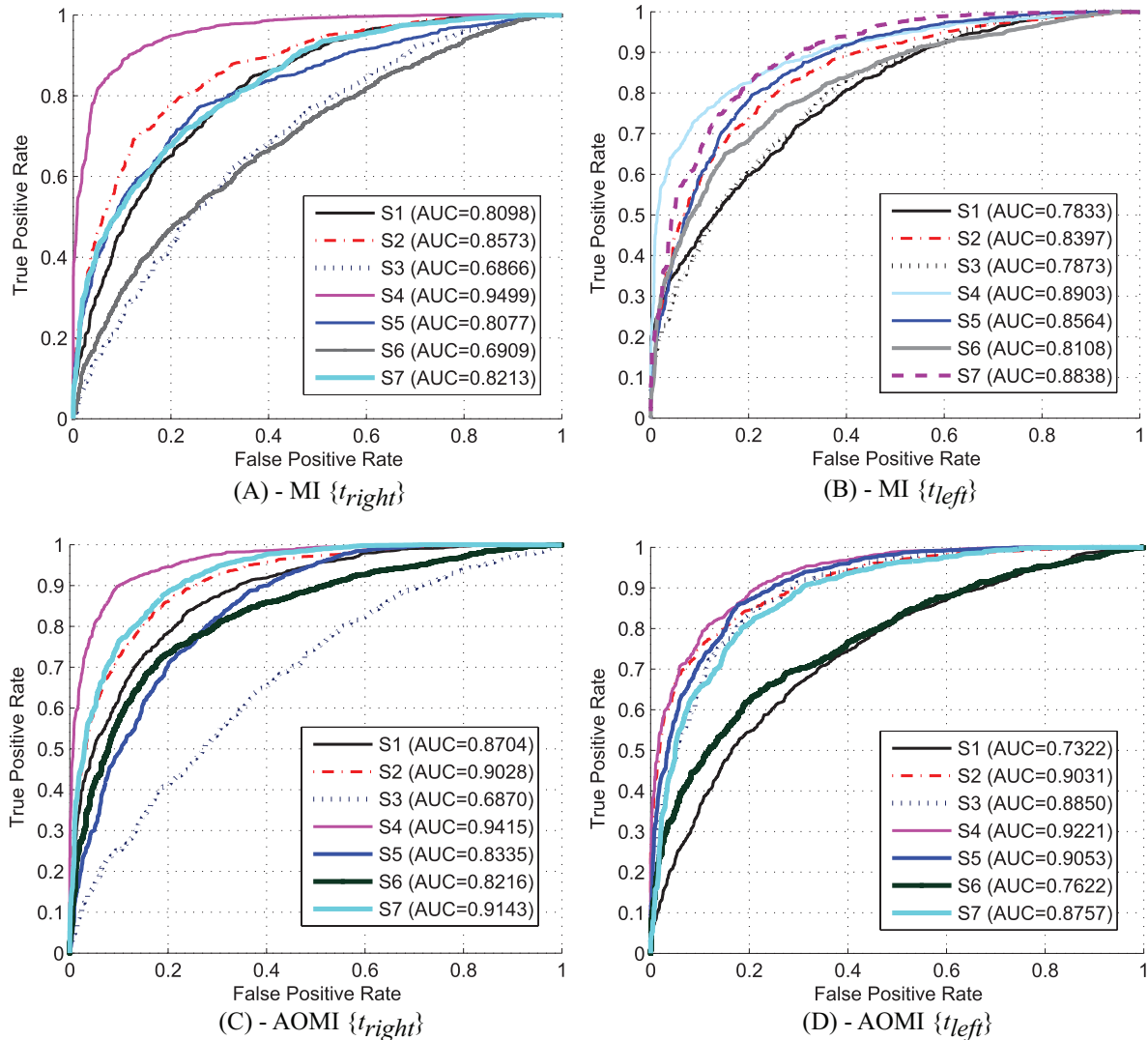


Fig. 4. Offline classification results from seven subjects for random test patterns. Plots (A) and (B) represent decoding of motor imagery (MI) tasks: (A) for  $\{t_{right}\}$  task, and (B) for  $\{t_{left}\}$  task. Plots (C) and (D) represent decoding of action observation-motor imagery (AOMI) tasks: (C) for  $\{t_{right}\}$ , and (D) for  $\{t_{left}\}$ . The value of AUC  $> 0.70$  is acceptable.

movement). In particular, for the rightward movement two subjects showed superior results:  $S4$ (AUC=0.9499) and  $S2$ (AUC=0.8573). In addition, three more subjects showed satisfactory results:  $S1$ (AUC=0.8098),  $S5$ (AUC=0.8077), and  $S7$ (AUC=0.8213). However, we noted inferior classifier performance for the remaining two subjects:  $S3$  (AUC=0.6866) and  $S6$  (AUC=0.6909). For the leftward movement, all subject showed satisfactory results, with three subjects  $S4$ ,  $S5$ , and  $S7$  showing superior results.

Inconsistency of results in the offline mode can be attributed to BCI intersession variability [47]. This problem of dramatic variability arises in neural signal measurements obtained during different recording sessions, even when the same subject is used. In addition, many other factors may affect the characteristics of neural signal measurements, resulting in variations. Such factors include the subject's condition, mood, fatigue, and drowsiness or even the subject's level of attention to a particular mental task [48].

We subsequently investigated AOMI task commands.

The plots of the decoding signal patterns are shown in Figs. 4C for the rightward task command, and Figs. 4D for the leftward task command. Significant improvements in AUC values with AOMI tasks were noticeable. For instance, superior results were observed for four subjects ( $S1$ ,  $S2$ ,  $S4$ , and  $S7$ ) in the rightward command task, with only one subject ( $S3$ ) that consistently remained with unsatisfactory results in the rightward command task. In addition, all subjects showed improved performance in AOMI compared to MI, with only one subject,  $S4$ , degrades by AUC=0.0084, but still showed superior results at AUC=0.9415. One subject,  $S6$ , the previously showed unsatisfactory results with MI now has a much better performance with an AUC=0.8216. For the leftward command task, all the subjects showed satisfactory results with four subjects ( $S2$ ,  $S3$ ,  $S4$ ,  $S5$ ) showing superior results. Degraded results showed for subjects  $S1$ ,  $S6$ , and  $S7$ , but remained within satisfactory results.

In summary, the offline results showed that our proposed

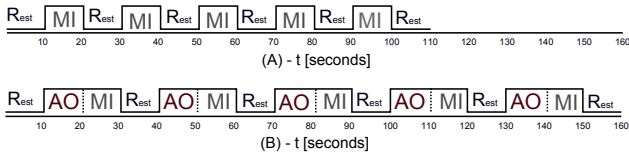


Fig. 5. Online experimental protocol for data acquisition. (A) Pure motor imagery (MI) task command. (B) Action observation-motor imagery (AOMI) task command. In both experiments, the classifiers decode a user’s intent every MI execution.

classification method in reading brain signal commands to move the haptic device leftward and rightward, has successfully achieved the desired motion at 25 out of 28 test cases with only three that showed unsatisfactory results. Furthermore, we observed that signal patterns using AOMI task commands produced better classification results than those using pure MI task commands. This offline analysis may seem uninformative so far. However, a more important aspect of our research is stable performance of the derived classification models during the real-time BCI experiments. In the next section we report the online results.

#### IV. ONLINE TEST RESULTS AND ANALYSIS

In this experiment, NIRS reads input brain signals from the subjects to move the haptic device in real-time. As in the offline case, we use both MI and AOMI task commands. Communication between NIRS and the haptic device is established through the user datagram protocol.

The online experimental steps are listed starting from Line 12 onwards of Algorithm 3. The input data defined in Line 12 correspond to streaming data given in real-time to the optimized classifiers. The final output command is attained on the basis of the AUC value. We conducted both experiments in at least five sessions, not exceeding one session per day or eight sessions in total for a given subject. The sessions were organized by inserting AO from the data acquisition protocol, shown in Fig. 3B. We set the timing of session blocks as shown in Fig. 5. The input consisted of test points 3-5 *sec* long for  $\mathcal{E}_1$  and  $\mathcal{E}_2$ , which were equivalent to 42 samples and 20 channels, that is,  $X \in R^{42 \times 20}$ . The classifier performance is measured during MI task execution periods as shown in Fig. 5.

1) *Experiment 1 (MI Task)*: Table 2 lists classification results from three different sessions corresponding to the pure MI task command. In general, lower classification accuracies were obtained in the online experiment than in the offline experiments. A strong variability is observed in the performances of classifiers across different subjects, sessions, and tasks. The mental tasks were more recognizable in some subjects than in other subjects, resulting in larger deviations in AUC values. Classifier performance in the  $\Theta_{accept}$  are shown in boldface, while  $\Theta_{worst}$  are italicised. The trained classifier was successful in 55 out of the total 63 cases with eight unacceptable cases.

On average, the classifier performances were equivalent to ( $AUC = 0.74 \pm 0.2$ ) within the  $\Theta_{accept}$  region. We obtained the maximum possible accuracy ( $AUC = 0.8441$ )

in classifying  $\{t_{left}\}$  data from Subject 4. It is noted that the case of  $\Theta_{best}$  performances were not consistent when classifying the same mental task by the same subject. This emphasizes the major BCI problem of inter-subject and inter-session variabilities with large standard deviations as shown in the table. Even if a participant performed well in one session, the performance within the session may have varied greatly among the  $\Theta_{best}$ ,  $\Theta_{accept}$  and  $\Theta_{worst}$  regions.

Let us consider the rest task  $\{t_{rest}\}$  in all three sessions. We note that during the first 3 *s* of a task period the classifiers produced increased false positive rates by detecting task-relevant signals as baseline signals. This is because of the high inherent latency of the brain hemodynamic response, which occurs over the interval 4-8 *s* after the task onset [4],[33]. Moreover, we have observed the occurrence of the  $U$  case in Eq. 4 when multiple classifiers did not detect any of the mental activity.

2) *Experiment 2 (AOMI Task)*: Table 3 lists the decoding results of signals corresponding to AOMI task commands. Compared to the MI task commands, AOMI task commands achieved superior accuracy. AOMI task commands were successful in 60 out of the total 63 cases with only three cases of failure.

Let us compare some specific results between MI and AOMI experiments. For instance, consider the Table 2 entries for Subject 1 during Session 2  $\{t_{right}\}$ , and Session 3  $\{t_{left}\}$  when the classifier accuracies were in the  $\Theta_{worst}$  region. In contrast, the corresponding entries of Table 3 show much improvement in the AUC values from the AOMI experiments.

By comparative analysis, we conclude the following. First, the average AUC values in the AOMI experiment were not significantly better than those of pure MI tasks. However, individual comparisons show improvements by subjects between sessions. Second, the standard deviations of AUC values were in a range similar to that of the last experiment. And lastly, the dominating inter-subject and inter-session variabilities were observed in terms of AUC values on both MI and AOMI experiments.

3) *Brain Mapping Analysis*: We assumed that the classifier performances were affected by the variability in the task-relevant cortical activation areas. Because the exact locations of the task-relevant channels were not always the same, we further analyzed a topographic cortical mapping of task-relevant oxy-Hb level changes by using a general linear model (GLM) algorithm explained in [42]. The significance thresholds for the statistical parametric maps were set to  $p < 0.05$ .

We separated the topographic map into nine regions of interest according to the functional anatomy of the premotor and prefrontal regions including the sensorimotor cortex (SMC), supplementary motor area (SMA), presupplementary motor area (preSMA), dorsal premotor cortex (PMC), and dorsolateral prefrontal cortex (PFC). The right lateral SMC was covered by Channels 1, 7, 8, and 9; the left lateral SMC by Channels 5, 6, 11, 12, and 13; the SMA by Channels 16, 17, 22, and 23; the preSMA by Channels

TABLE II  
EXPERIMENT 1: THE ONLINE PERFORMANCE OF CLASSIFIERS IN DECODING SIGNALS CORRESPONDING TO PURE MOTOR IMAGERY (MI) TASK  
COMMANDS OF  $\{t_{right}\}$ ,  $\{t_{left}\}$ , AND  $\{t_{rest}\}$ .

Subjects	Session 1			Session 2			Session 3		
	$\{t_{right}\}$ (AUC)	$\{t_{left}\}$ (AUC)	$\{t_{rest}\}$ (AUC)	$\{t_{right}\}$ (AUC)	$\{t_{left}\}$ (AUC)	$\{t_{rest}\}$ (AUC)	$\{t_{right}\}$ (AUC)	$\{t_{left}\}$ (AUC)	$\{t_{rest}\}$ (AUC)
Subject 1	0.7781	<b>0.8101</b>	0.1824	0.6987	0.7754	0.1624	0.7141	0.6998	0.2811
Subject 2	<b>0.8115</b>	0.6755	0.3045	0.7375	0.6589	0.1847	0.7157	<b>0.8095</b>	0.1450
Subject 3	0.7801	0.7787	0.2104	0.7584	<b>0.8201</b>	0.1279	0.6590	0.7189	0.2515
Subject 4	0.7124	<b>0.8441</b>	0.1980	<b>0.8014</b>	0.7352	0.1848	0.7684	0.7871	0.2801
Subject 5	<b>0.8380</b>	0.7600	0.1709	0.7412	0.7278	0.2812	0.6971	0.7358	0.2103
Subject 6	0.7312	0.7112	0.1782	0.7813	0.7177	0.2104	0.7300	0.7784	0.2081
Subject 7	0.6819	0.7211	0.1541	0.7987	<b>0.8380</b>	0.1784	0.7630	0.6798	0.2765
<b>Mean</b>	0.7618	0.7572	0.1997	0.7596	0.7533	0.1899	0.7210	0.7441	0.2360
<b>S.D.</b>	0.0557	0.0590	0.0496	0.0371	0.0622	0.0475	0.0378	0.0484	0.0509

TABLE III  
EXPERIMENT 2- THE ONLINE PERFORMANCE OF CLASSIFIERS IN DECODING SIGNALS CORRESPONDING TO ACTION OBSERVATION-MOTOR  
IMAGERY (AOMI) TASKS COMMANDS OF  $\{t_{right}\}$ ,  $\{t_{left}\}$  AND  $\{t_{rest}\}$ .

Subjects	Session 1			Session 2			Session 3		
	$\{t_{right}\}$ (AUC)	$\{t_{left}\}$ (AUC)	$\{t_{rest}\}$ (AUC)	$\{t_{right}\}$ (AUC)	$\{t_{left}\}$ (AUC)	$\{t_{rest}\}$ (AUC)	$\{t_{right}\}$ (AUC)	$\{t_{left}\}$ (AUC)	$\{t_{rest}\}$ (AUC)
Subject 1	<b>0.8103</b>	0.7811	0.1441	0.7217	<b>0.8125</b>	0.1341	<b>0.8974</b>	0.7489	0.1481
Subject 2	0.7357	0.6982	0.2105	0.7875	0.7510	0.1671	<b>0.8300</b>	0.7712	0.1901
Subject 3	0.7508	0.7517	0.2100	0.8780	0.7982	0.1569	0.7124	0.7680	0.2074
Subject 4	<b>0.8142</b>	0.7802	0.1870	0.7984	0.6815	0.1908	<b>0.8670</b>	0.7046	0.2011
Subject 5	0.7918	0.6901	0.2650	0.7550	0.7201	0.2233	0.7919	<b>0.9308</b>	0.1030
Subject 6	<b>0.8301</b>	0.7011	0.1982	<b>0.8183</b>	0.7870	0.1789	0.7710	0.7118	0.1900
Subject 7	0.7416	0.7809	0.1455	0.7004	0.7909	0.1399	0.7321	0.7808	0.1987
<b>Mean</b>	0.7820	0.7407	0.1923	0.7799	0.7630	0.1701	0.8002	0.7737	0.1769
<b>S.D.</b>	0.0387	0.04255	0.0417	0.0603	0.0477	0.0309	0.0683	0.0752	0.0379

35, 36, 42, and 43; the right PMC by Channels 14, 15, 20, and 28; the left PMC by Channels 18, 19, 24, 25, and 26; the left PFC by Channels 27, 33, 34, 40, and 41; and the right PFC by Channels 31, 32, 37, 38, 39, 44, and 45.

The location of a Cz reference point is represented by Channel 10 (see Fig. 2(A)). Fig. 5 shows a distinct cortical activation pattern reconstructed from data on Subject 1 across different sessions for both MI and AOMI tasks. Task-relevant increases of oxy-Hb were prominent in the prefrontal regions but were strongly dependent on the task type and the session type. For instance, with repetition of the session the increase of oxy-Hb appeared to intensify for the channels covering the right and left PMC for both MI and AOMI while performing the  $\{t_{left}\}$  task. The oxy-Hb was augmented in the channels covering the SMA and remained unchanged in the channels covering the left SMC. For the MI-based  $t_{right}$  task, we have observed the reverse case; that is, with repetition of the session the oxy-Hb concentration levels were observed to decrease in the pre-

SMA and PFC regions. By using Algorithm2 each time, we tend to select for a classifier only those task-relevant channels with higher activations. Therefore, each time the locations of task-relevant channels vary, the performance of a classifier is affected. In general, cortical activation in the pre-SMA and PFC remained relatively unchanged among most of the subjects within a session. We visually inspected all changes in the regional activation with respect to the subject, task, and session type.

We briefly summarize our findings of the mapping analysis as follows:

- A session-dependent cortical activation was seen for both MI and AOMI tasks.
- In some subjects, the cortical activation levels increased with the number of sessions.
- The AOMI task produced higher cortical activation than the MI task. The major activation locations for the AOMI task included the PFC, PMC, SMA, and pre-SMC regions.



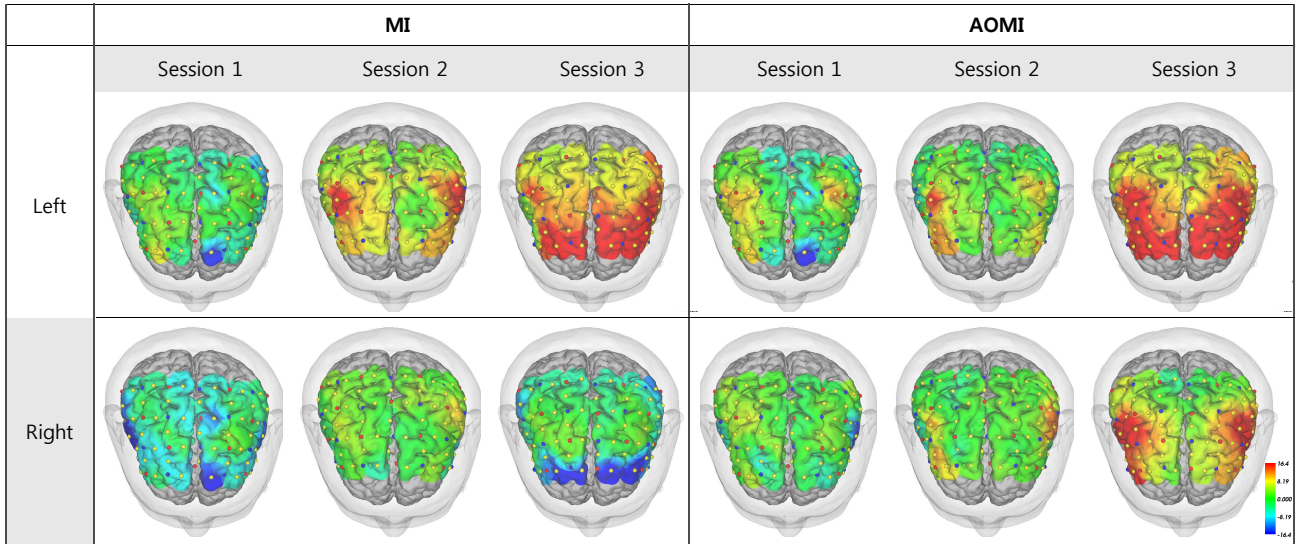


Fig. 6. Representative cortical mapping of oxy-Hb level changes related to MI and AOMI tasks. The data were obtained from Subject 1 over three sessions. The color scale indicates the coordinates of concentration changes in oxy-Hb with t-values.

- The effect size calculated by using oxy-Hb levels showed no significant difference in either the  $\{t_{right}\}$  ( $p = 0.203$ ) or the  $\{t_{left}\}$  ( $p = 0.535$ ). In terms of the course of oxy-Hb changes during the AOMI period, two tasks showed comparable intervals between the start of the  $\{t_{right}\}$  task and the peak of oxy-Hb in the  $\{t_{left}\}$ .
- No strong correlation between the MI and AOMI tasks was observed. The effect of preparation on the increases in oxy-Hb level during the MI task and AOMI task was evaluated by calculating effect sizes. In terms of oxy-Hb levels, a one-way ANOVA showed a significant main effect for site during both the MI period ( $p < 0.05$ ) and in the AOMI period ( $p < 0.05$ ).

## V. DISCUSSION

We have shown that it is possible to command a haptic device to move in opposing directions by detecting oxy-Hb signal reading from NIRS-BCI system. This study proposes that such capability can be used for neurorehabilitation to induce brain plasticity for stroke patients, or possibly provide them with some degree of self-sufficiency. MI and AOMI task commands were implemented in both online and offline modes. Feature extraction and channel localization reduced noise in the input signals for classification of multiple SVMs. The online BCI classification of pure motor imagery tasks was 76% accurate on average. And we observed a significant improvement in the BCI accuracies of up to 93% when using signals from AOMI task compared to pure MI. Compared to other studies, ours has obtained improved classification rates, as shown in Table 4. Note that only a few online classification results achieved performances in the range of 70%-90% [57], [51]. Except for the results of Abdelnour et al. [49] whose online classification rate ranges from 68.8% to 100%, our work showed better results. However, it is noted that [49] used

real finger tapping which is more discriminable than pure mental task.

The methodology proposed in this paper differs from that in the other studies by virtue of the following attributes:

- We use 45-channels recordings which cover the most important regions of the brain cortex (SMC, SMA, and PFC). This is in contrast with other NIRS-BCI methods, which usually cover minimal locations of the brain cortex. We then perform an automated channel selection method which allowed us to localize 20 most task relevant channels for subsequent classification. Using multiple channels can be seen as a disadvantage, in general. However, our motivation was to accurately localize task relevant channels each time when subjects perform a specific mental task. Further, because we conduct two different experiments with new tasks (the imaginary directional movement tasks are not common BCI research) there was a need to investigate multiple channel recordings. Moreover, before each online experiment we perform a channel localization within minutes in each session and for each subject. Such localization helps to capture the session or subject specific neural activation within the few relevant channels. For instance, we have noticed that the classifier uses different channel combinations to discriminate between the imaginary rightward movement and the imaginary leftward movement. In case the fixed number of channels over a specific brain region were used then the classification accuracy could be very unsatisfactory. This is a different mechanism which allowed us to automatically switch the strong task relevant channels among various mental tasks.
- We performed different BCI experiments that included directional hand movement tasks based on pure motor imagery (MI) tasks and combined action observation and motor imagery (AOMI) tasks. We found that

TABLE IV  
ANALYSIS METHODS USED IN PREVIOUS NIRS-BCI STUDIES. THE ASTERISKS DENOTE ONLINE CLASSIFICATION RESULTS

Author (Ref)	Brain region	Input features	Classifier	Performance
<b>Our study</b>	Prefrontal, Sensorimotor cortex	OxyHb PCA	Ensemble SVM Classifiers	<b>76%-93%*</b>
Abdelnour ([49])	Motor cortex	OxyHb after Kalman filtering	Linear discriminant analysis (LDA)	68%-100%*
Coyle ([50])	Motor cortex	mean OxyHb	OxyHb amplitude threshold detector	80%*
Utsugi ([51])	Prefrontal cortex	OxyHb	Artificial Neural Networks	70%-90%*
Abibullaev ([40])	Prefrontal cortex	OxyHb wavelet coefficients	Linear discriminant analysis , Artificial Neural Networks, SVM	LDA 81%-95%, ANN 69%-91% SVM 94%-97%
Coyle ([3])	Motor cortex	mean OxyHb of 20sec data	Simple threshold detector	75%
Cui ([52])	Motor cortex	different features OxyHb, deOxyHb	Support Vector Machines	70% - 90%
Fazli ([53])	Prefrontal, Motor cortex	EEG& fNIRS Hybrid features	Linear Discriminant Analysis	78.6%-92.9%
Sassaroli ([54])	Prefrontal cortex	OxyHb, deOxyHb raw features	K-means algorithm	55.6%-72.2%
Sitaram ([13])	Frontal cortex	OxyHb intensity	Hidden Markov Models (HMM), SVM	SVM 73% HMM 89%
Tai ([55])	Prefrontal cortex	OxyHb intensity	LDA, SVM	75%-96%
Truong ([56])	Prefrontal cortex	OxyHb wavelet decomposition	Artificial Neural Networks (ANN)	95%

AOMI tasks were more classifiable compared to the pure MI tasks. Our idea of designing the directional movement tasks are intended for application in stroke rehabilitation physical therapy, which is envisaged to combine BCI with therapeutic devices for upper limb exercises. We have extracted the tasks after reviewing the important tasks used in stroke rehabilitation to improve the activities of daily living (ADL). The example of other tasks include "reaching", "pulling", "flexion" and "extension" of upper limb. Among them in our initial phase we implemented "leftward" and "rightward" movements. The haptic device was just a test platform, however it can be easily replaced with the available upper limb physical therapy devices (e.g. MIT Manus). The limitation of our study is that we study only normal subjects at present study. Moreover, the number of subjects are limited to seven. Because our initial goal was to verify the feasibility of our BCI approach. Nonetheless, we measured the data from extensive number of sessions to support the potential of the present approach. Another important question is that whether the AOMI task is effective for effective neuro-rehabilitation (e.g. improved cortical re-organization or neuroplasticity). We focus to study these question in our future study. Due to the possible application of our study, we put higher priority in the detection of MI tasks in a direct (non-interpretive) way

to provide natural BCI outputs.

- We presented a different classification approach which is robust against the major BCI classification problems. Because we have optimized the classifiers in the offline settings from vast data from as many sessions as possible, they performed robust throughout online experiments. There were only few exceptions of lower classification results. To date, most NIRS-BCI studies used standard classifiers such as SVMs, LDA, HMM, or ANNs from Table 3. This study presents another classifier which achieves higher accuracies by using a multiple learning strategy. However, it is not appropriate to compare and judge the research results in terms of classification accuracy, because many factors influence the difficulty and the accuracy in a particular BCI study. For instance, such factors include the type of BCI paradigm and whether the NIRS signal characteristics used are raw, preprocessed, or transformed. In addition, the type of the system used to acquire the NIRS signals is a factor. In our study, the signal sampling frequency was 14.28 Hz, whereas other NIRS-BCIs use signals with sampling rates from 2 Hz to 10 Hz. The lower the sampling frequency, the lower the signal quality and harder the extraction of the true neural signals from background noise.

One known limitation of the present NIRS-BCI approach is the delay in operating a haptic device because of the

intrinsic latency of the brain hemodynamics. With an EEG-BCI system, an operation can be performed over a few milliseconds. We plan to experiment two possible ways of overcoming the slowness of the NIRS-BCI that we aim to research in the next step. The first is based on exploring fast hemodynamic responses as was done by Cui et al. (2010). The other is to develop a hybrid BCI paradigm that combines EEG and NIRS signals for rapid detection of mental state as in (Fazli et al., 2012). In addition, we plan to extensively study the influence of the various feedback types (visual, auditory, or haptic) and their effects on the improvement of the overall classification accuracies. In general, the NIRS-BCI may not be suitable for a fast translation of mental intent, however we believe that it has potential for a neurorehabilitation and motor learning of post-stroke patients that involves slow operations.

## REFERENCES

- [1] G. Pfurtscheller, G. Müller-Putz, R. Scherer, and C. Neuper, "Rehabilitation with brain-computer interface systems," *Computer*, vol. 41, no. 10, pp. 58–65, 2008.
- [2] M. Grosse-Wentrup, D. Mattia, and K. Oweiss, "Using brain-computer interfaces to induce neural plasticity and restore function," *J. Neural Eng.*, vol. 8, no. 2, p. 025004, 2011.
- [3] S. Coyle, T. Ward, C. Markham, and G. McDarby, "On the suitability of near-infrared (NIR) systems for next-generation brain-computer interfaces," *Physiol. Meas.*, vol. 25, pp. 815–822, 2004.
- [4] E. Coffey, A. Brouwer, E. Wilschut, and B. Jan, "Brain-machine interfaces in space: Using spontaneous rather than intentionally generated brain signals," *Acta Astronautica*, vol. 67, no. 1, pp. 1–11, 2010.
- [5] F. Matthews, B. Pearlmutter, T. Ward, C. Soraghan, and C. Markham, "Hemodynamics for brain-computer interfaces," *IEEE Signal Processing Magazine*, vol. 25, pp. 87–94, 2009.
- [6] Q. Zhang, G. Strangman, and G. Ganis, "Adaptive filtering to reduce global interference in non-invasive NIRS measures of brain activation: How well and when does it work?" *Neuroimage*, vol. 45, no. 3, pp. 788–94, 2009.
- [7] J. An, S.H. Lee, S.H. Jin, B. Abibullaev, "The beginning of neuro-haptics: Controlling cognitive interaction via brain haptic interface," *Brain-Computer Interface (BCI), 2013 International Winter Workshop on*, pp. 103–106, 18–20 Feb. 2013.
- [8] B. Abibullaev, J. An, S.H. Jin, S.H. Lee, J.I. Moon, "Minimizing inter-subject variability in fNIRS-based brain-computer interfaces via multiple-kernel support vector learning," *Med Eng Phys*, vol. 35, pp. 1811–8, 2013.
- [9] B. Abibullaev, J. An, S.H. Jin, J.I. Moon, "Classification of brain hemodynamic signals arising from visual action observation tasks for brain-computer interfaces: A functional near-infrared spectroscopy study," *Measurement*, vol. 49, pp. 320–328, 2014.
- [10] A. Nijholt and D. Tan, "Brain-computer interfacing for intelligent systems," *Intelligent Systems, IEEE*, vol. 23, no. 3, pp. 72–79, 2008.
- [11] L. Marchal-Crespo and D. J. Reinkensmeyer, "Review of control strategies for robotic movement training after neurologic injury," *Journal of NeuroEngineering and Rehabilitation*, vol. 6, no. 20, pp. 1–15, 2009.
- [12] R. Krepki, G. Curio, B. Blankertz, and K.-R. Müller, "Berlin brain-computer interface – the hci communication channel for discovery," *International Journal of Human-Computer Studies*, vol. 65, no. 5, pp. 460 – 477, 2007.
- [13] R. Sitaram, H. Zhang, C. Guan, M. Thulasidas, Y. Hoshi, A. Ishikawa, K. Shimizu, and N. Birbaumer, "Temporal classification of multichannel near-infrared spectroscopy signals of motor imagery for developing a brain-computer interface," *Neuroimage*, vol. 34, pp. 1416–27, 2007.
- [14] R. Dickstein and J. E. Deutsch, "Motor imagery in physical therapy practice," *Physical Therapy*, vol. 87, no. 7, pp. 942–953, July 2007.
- [15] K. Jerbi, J. Vidal, J. Mattout, E. Maby, F. Lecaigard, T. Ossando, C. Hamamé, S. Dalal, R. Bouet, and J.-P. Lachaux, "Inferring hand movement kinematics from the MEG, EEG and intracranial EEG: From brain-machine interfaces to motor rehabilitation," *IRBM*, vol. 32, no. 1, pp. 8–18, 2009.
- [16] C. J. Bohil, B. Alicea, and F. A. Biocca, "Virtual reality in neuroscience research and therapy," *Nature Reviews Neuroscience*, vol. 12, no. 12, pp. 752–762, Dec. 2011.
- [17] B. Lance, S. Kerick, A. Ries, K. Oie, and K. McDowell, "Brain-computer interface technologies in the coming decades," *Proceedings of the IEEE*, vol. 100, no. Special Centennial Issue, pp. 1585–1599, May 2012.
- [18] S. Machado, F. Araujo, F. Paes, B. Velasques, M. Cunha, H. Budde, L. Basile, R. Anghinah, O. Arias-Carrion, M. Cagy, R. Piedade, T. Graaf, A. Sack, and P. Ribeiro, "EEG-based brain-computer interfaces: An overview," *Reviews in the Neurosciences*, vol. 21, no. 6, pp. 451–468, Oct. 2010.
- [19] J. J. Shih, D. J. Krusienski, and J. R. Wolpaw, "Brain-computer interfaces in medicine," *Mayo Clinic Proceedings*, vol. 87, no. 3, pp. 268 – 279, 2012.
- [20] D. Mattia, F. Pichiorri, M. Molinari, and R. Rupp, "Brain computer interface for hand motor function restoration and rehabilitation," in *Towards Practical Brain-Computer Interfaces*, ser. Biological and Medical Physics, Biomedical Engineering, B. Z. Allison, S. Dunne, R. Leeb, J. Del R. Millán, and A. Nijholt, Eds. Springer Berlin Heidelberg, 2013, pp. 131–153.
- [21] O. Bai, P. Lin, D. Huang, D.-Y. Fei, and M. K. Floeter, "Towards a user-friendly brain-computer interface: initial tests in ALS and PLS patients," *Clinical Neurophysiology: Official Journal of the International Federation of Clinical Neurophysiology*, vol. 121, no. 8, p. 1293, 2010.
- [22] E. Buch, C. Weber, L. G. Cohen, C. Braun, M. A. Dimyan, T. Ard, J. Mellinger, A. Caria, S. Soekadar, A. Fourkas, and N. Birbaumer, "Think to move: a neuromagnetic brain-computer interface (BCI) system for chronic stroke," *Stroke*, vol. 39, no. 3, pp. 910–917, 2008.
- [23] M. Palankar, K. De Laurentis, R. Alqasemi, E. Veras, R. Dubey, Y. Arbel, and E. Donchin, "Control of a 9-dof wheelchair-mounted robotic arm system using a P300 brain computer interface: Initial experiments," in *Robotics and Biomimetics, 2008. ROBIO 2008. IEEE International Conference on*, 2009, pp. 348–353.
- [24] A. S. Merians, E. Tunik, and S. V. Adamovich, "Virtual reality to maximize function for hand and arm rehabilitation: exploration of neural mechanisms," *Studies in Health Technology and Informatics*, vol. 145, pp. 109–125, 2009.
- [25] I. K. Niazi, N. Jiang, O. Tiberghien, J. Nielsen, K. Dremstrup, and D. Farina, "Detection of movement intention from single-trial movement-related cortical potentials," *Journal of Neural Engineering*, vol. 8, no. 6, p. 066009, 2011.
- [26] A. Ramos-Murguialday, M. SchÄijrholz, V. Caggiano, M. Wildgruber, A. Caria, E. M. Hammer, S. Halder, and N. Birbaumer, "Proprioceptive feedback and brain computer interface (BCI) based neuroprostheses," *PLoS ONE*, vol. 7, no. 10, p. e47048, 10 2012.
- [27] A. Murguialday, E. Soares, and N. Birbaumer, "Upper limb emg artifact rejection in motor sensitive bcis," in *Engineering in Medicine and Biology Society (EMBC), 2010 Annual International Conference of the IEEE*, 2010, pp. 1–6.
- [28] K. K. Ang, C. Guan, C. Wang, K. S. Phua, A. Tan, and Z. Y. Chin, "Calibrating eeg-based motor imagery brain-computer interface from passive movement," in *Engineering in Medicine and Biology Society, EMBC, 2011 Annual International Conference of the IEEE*, 2011, pp. 4199–4202.
- [29] T. Meyer, J. Peters, D. Brtz, T. Zander, B. Scholkopf, S. Soekadar, and M. Grosse-Wentrup, "A brain-robot interface for studying motor learning after stroke," in *Intelligent Robots and Systems (IROS), 2012 IEEE/RSJ International Conference on*, 2012, pp. 4078–4083.
- [30] R. Zimmermann, L. Marchal-Crespo, J. Edelmann, O. Lambercy, M.-C. Fluet, R. Riener, M. Wolf, R. Gassert et al., "Detection of motor execution using a hybrid fNIRS-biosignal BCI: a feasibility study," *Journal of NeuroEngineering and Rehabilitation*, vol. 10, no. 1, p. 4, 2013.
- [31] M. Gomez-Rodriguez, J. Peters, J. Hill, B. Schölkopf, A. Gharabaghi, and M. Grosse-Wentrup, "Closing the sensorimotor loop: haptic feedback facilitates decoding of motor imagery," *J. Neural Eng.*, vol. 8, no. 3, p. 036005, 2011.
- [32] A. Chatterjee, V. Aggarwal, A. Ramos, S. Acharya, and N. Thakor, "A brain-computer interface with vibrotactile biofeedback for haptic information," *J. Neuroeng. Rehab.*, vol. 4, no. 1, p. 40, 2007.

- [33] E. Gratton, V. Toronov, U. Wolf, M. Wolf, and A. Webb, "Measurement of brain activity by near-infrared light," *J. Biomed. Opt.*, vol. 10, no. 1, p. 011008, 2005.
- [34] M. Jueptner and C. Willer, "Does measurements of regional cerebral blood flow reflects synaptic activity? - implications for PET and fMRI," *NeuroImage*, vol. 2, pp. 148–156, 1995.
- [35] J. Jarvelainen, M. Schurmann, and R. Hari, "Activation of the human primary motor cortex during observation of tool use," *NeuroImage*, vol. 23, pp. 187–192, 2004.
- [36] D. Tkach, J. Reimer, and N. Hatsopoulos, "Congruent activity during action and action observation in motor cortex," *J of Neurosci*, vol. 27, no. 48, pp. 13 241–13 250, 2007.
- [37] J. Virtanen, T. Noponen, and P. Merilainen, "Comparison of principal and independent component analysis in removing extracerebral interference from near-infrared spectroscopy signals," *J Biomed Opt*, vol. 14, no. 5, p. 054032, 2009.
- [38] M. Izzetoglu, A. Devaraj, A. Bunce, and B. Onaral, "Motion artifact cancellation in NIR spectroscopy using wiener filtering," *IEEE Transactions on Biomedical Engineering*, vol. 52, pp. 934–38, 2005.
- [39] K. Jang, S. Tak, J. Jung, Y. Jeong, and J. Ye, "Wavelet minimum description length detrending for near-infrared spectroscopy," *J. Biomed. Opt.*, vol. 14, pp. 034 004–13, 2009.
- [40] B. Abibullaev and J. An, "Classification of frontal cortex haemodynamic responses during cognitive tasks using wavelet transforms and machine learning algorithms," *Med. Eng. Phys.*, vol. 34, no. 10, pp. 1394–410, 2012.
- [41] L. Lal, M. Schroder, T. Hinterberger, J. Weston, M. Bogdan, N. Birbaumer, and B. Scholkopf, "Support vector channel selection in BCI," *IEEE Transactions on Biomedical Engineering*, vol. 51, no. 6, pp. 1003–1010, 2009.
- [42] M. Schroeter, M. Bucheler, K. Muller, K. Uludag, H. Obrig, and G. Lohmann, "Towards a standard analysis for functional near-infrared imaging," *NeuroImage*, vol. 21, pp. 283–90, 2004.
- [43] M. Schroder, T. Lal, T. Hinterberger, M. Bogdan, N. Hill, N. Birbaumer, W. Rosenstiel, and B. Scholkopf, "Robust EEG channel selection across subjects for brain-computer interfaces," *EURASIP J. Appl. Signal Process.*, vol. 19, pp. 3103–3112, 2005.
- [44] I. Guyon, J. Weston, S. Barnhill, and V. Vapnik, "Gene selection for cancer classification using support vector machines," *Mach. Learn.*, vol. 4, no. 1, pp. 389–422, 2002.
- [45] B. Scholkopf and A. Smola, *Learning with Kernels, Support Vector Machines, Regularization, Optimization, and Beyond*. MIT Press, Cambridge, 2002.
- [46] A. Bradley, "The use of the area under the ROC curve in the evaluation of machine learning algorithms," *Pattern Recogn.*, vol. 30, pp. 1145–1159, 2009.
- [47] M. Gerven, J. Farquhar, R. Schaefer, R. Vlek, J. Geuze, A. Nijholt, N. Ramsey, P. Haselager, L. Vuurpijl, S. Gielen, and P. Desain, "The brain-computer interface cycle," *J. of Neural Eng.*, vol. 6, no. 4, pp. 1–9, 2009.
- [48] B. Blankertz, F. Losch, M. Krauledat, G. Dornhege, G. Curio, and K. Muller, "The Berlin brain-computer interface: Accurate performance from first-session in BCI-naive subjects," *IEEE Transactions on Biomedical Engineering*, vol. 55, pp. 2452–2462, 2008.
- [49] A. Abdelnour and T. Huppert, "Real-time imaging of human brain function by near-infrared spectroscopy using an adaptive general linear model," *NeuroImage*, vol. 46, pp. 133–143, 2009.
- [50] S. Coyle, T. Ward, and C. Markham, "Physiological noise in near-infrared spectroscopy: implications for optical brain computer interfacing," in *26th Annual Int. Conf. of the IEEE Eng. in Med. and Biol. Soc.*, vol. 2, 2004, pp. 4540–4543.
- [51] K. Utsugi, A. Obata, H. Sato, T. Katsura, K. Sagara, A. Maki, and H. Koizumi, "Development of an optical brain-machine interface," in *Proc IEEE EMBS Lyon France, 2007*, pp. 5338–5341.
- [52] X. Cui, S. Bray, and A. Reiss, "Speeded near infrared spectroscopy response detection," *PLoS ONE*, vol. 5, no. 11, p. e15474, 2010.
- [53] S. Fazli, J. Mehnert, J. Steinbrink, G. Curio, A. Villringer, K. Muller, and B. Blankertz, "Enhanced performance by a hybrid NIRS-EEG brain computer interface," *NeuroImage*, vol. 59, no. 1, p. 519:29, 2012.
- [54] A. Sassaroli, F. Zheng, L. Hirshfield, A. Girouard, E. Solovey, R. Jacob, and S. Fantini, "Discrimination of mental workload levels in human subjects with functional near-infrared spectroscopy," *J. Innov. Opt. Health. Sci.*, vol. 1, no. 2, pp. 227–37, 2008.
- [55] K. Tai and T. Chau, "Single-trial classification of NIRS signals during emotional induction tasks: Towards a corporeal machine interface," *J. Neuroeng. Rehabil.*, vol. 9, pp. 9–39, 2009.
- [56] Q. Truong and N. Masahiro, "Functional near infrared spectroscopy for cognition brain tasks by wavelets analysis and neural networks," *Int. J. of Biomed. Med. Sci.*, vol. 4, no. 1, pp. 28–33, 2009.
- [57] S. Coyle, T. Ward, and C. Markham, "Brain-computer interface using a simplified functional near-infrared spectroscopy system," *J. of Neural Eng.*, vol. 4, pp. 219–26, 2007.